10

Spin-Polarized Scanning Tunneling Spectroscopy

M. Bode and R. Wiesendanger

Within recent years spin-polarized scanning tunneling spectroscopy (SP-STS) has developed into a mature tool for ultrahigh spatial resolution magnetic domain imaging. In this chapter, we will introduce the measurement principle of SP-STS and describe experimental procedures and requirements. We will discuss present data measured on different ferro- and antiferromagnetic sample systems demonstrating the particular strength of SP-STS, i.e., the ability for simultaneous observation of structural, electronic, and magnetic properties.

10.1 Introduction

As already described in the previous chapter, spin-polarized electron tunneling in planar tunnel junctions has been a well established experimental technique since the early 1970s [1,2]. The power of persuasion of these first experiments was based on an appropriate choice of electrode materials, i.e., a ferromagnetic and superconducting electrode, in combination with the use of spectroscopic techniques.

The planar tunnel junctions were fabricated by growing a thin ferromagnetic film on an oxidized, self-passivating aluminum sample. The thin layer of aluminum oxide served as a tunneling barrier. In particular, the electronic properties of the superconductor (aluminum at $T = 0.3\ K$) played an important role. Close to the Fermi level its quasiparticle density of states (DOS) is dominated by two peaks separated by a small gap with a width of a few meV. If exposed to a strong external field, the Zeeman energy leads to an additional well-defined spin splitting of both peaks leading to four peaks, two of which exhibit a polarization parallel to the magnetization of the ferromagnet and two of which exhibit an antiparallel orientation. Therefore, the spin-polarized electronic structure of the superconductor is known from elementary physical principles, and any spin-polarized contribution to the tunneling current will lead to a predictable asymmetry in the tunneling spectra.

Indeed, Tedrow et al. [1,2] observed strongly asymmetric spectra when the counter electrode was made of a ferromagnetic material, which clearly proved the spin polarization of the tunneling current. A quantitative analysis allowed the calculation

of the degree of spin polarization and revealed significant discrepancies when compared with clean single-crystalline ferromagnetic surfaces. These discrepancies are, however, not surprising since the electronic structure of ferromagnetic surfaces is certainly modified by the presence of the tunneling barrier, mostly made of AlO_2, and by the roughness of the interface.

These seminal experiments performed by Tedrow et al. [1, 2] show exemplarily how to overcome the main problems of spin-polarized scanning tunneling microscopy (SP-STM), i.e., the clear identification of a spin-polarized signal and the separation of topographic, electronic, and magnetic contributions. In direct analogy to those experiments, one could use a superconducting probe tip. However, the experimental setup must be exposed to a strong external magnetic field in order to achieve a sufficiently high Zeeman splitting, which will destroy the remanent domain structure and saturate the magnetization of the sample. Therefore, the use of superconducting tips may be useful for a quantitative analysis of the spin polarization of clean surfaces, but it is certainly not practicable for imaging magnetic domains.

As originally proposed by Pierce [3], optically pumped semiconducting or ferromagnetic probe tips may be used alternatively. Actually, optically pumped GaAs is routinely used as a source of spin-polarized electrons. By making use of the spin splitting of the GaAs valence band, the illumination of a GaAs tip with circularly polarized light may lead to some spin sensitivity. This experimental setup is particularly promising since no magnetic materials are involved, which excludes any unwanted modification of the sample's magnetic domain structure. Although this approach toward spin-sensitive STM has been followed in several laboratories [4–6], magnetic imaging has not yet been demonstrated unambiguously. Possibly, the problems, at least in part, are caused by the fact that due to the geometry of the tunnel junction, which is formed by the more or less flat sample and the pyramidally shaped tip, the polarization of the incident light at the apex of the probe tip is rather unpredictable. Furthermore, it may vary depending on the actual position of the tip with respect to the sample.

Alternatively, the intrinsic spin imbalance of (ferro)magnetic materials may be used for spin-sensitive experiments. Different procedures have been proposed in the past in order to avoid the tip's magnetic stray field modifying or even destroying the domain structure of the sample to be investigated. In the previous chapter, it was shown that bulk magnetic samples can be imaged with amorphous magnetic materials that exhibit an extremely low saturation magnetization. This experimental approach is, however, probably not suitable for the investigation of thin magnetic films. Instead, we have minimized the magnetic stray field by utilizing nonmagnetic probe tips that were coated by an ultrathin layer (typically a few atomic layers) of magnetic material. In the following, we will briefly describe the experimental setup and procedures. Then we will explain the contrast mechanism of spin-polarized scanning tunneling spectroscopy by making use of the exchange-split surface state of ferromagnetic Gd(0001), which represents an analogue to the Zeeman-split DOS of a superconductor in a strong external magnetic field. Then we will demonstrate the scientific impact of SP-STS on three different test samples: The ability of SP-STS to image magnetic domains and domain walls with a spatial resolution well below

1 nm has been demonstrated on ferromagnetic Fe nanowires [7]. Furthermore, the extremely high surface sensitivity of SP-STS allows the magnetic imaging of layered antiferromagnets as, e.g., Cr(001). Finally, we will show that atomic spin resolution can be achieved on the densely packed antiferromagnetic surface of a Mn monolayer on W(110) in the constant-current mode.

10.2 Experimental Setup

All experiments described in this section have been performed under UHV conditions, i.e., neither for the preparation of the sample nor the tip has the vacuum been broken. Up until now, different kinds of scanning tunneling microscopes have been used for SP-STM, commercially available and home-built, operated at room, variable, or low temperatures. Common to all microscopes is the absence of strong permanent magnetic fields at the sample location and a reliable tip exchange mechanism that allows the use of in-situ cleaned and coated probe tips [8].

Obviously, a proper tip preparation is an essential requirement for performing SP-STM experiments. Currently, we are using tungsten tips that are coated by a thin layer of ferromagnetic material. The tungsten tips are prepared by etching a polycrystalline wire in saturated NaOH solution (8 g NaOH/100 ml H_2O). This etching procedure results in tips with a typical diameter of 20 – 50 nm. After introduction into the UHV system, the tips are heated to at least 2200 K in order to remove oxide and other contaminants. This preparation procedure does not change the general shape of the tip, but causes the apex of the tip to become blunt, as can be seen in the scanning electron microscope (SEM) images shown in Fig.10.1.

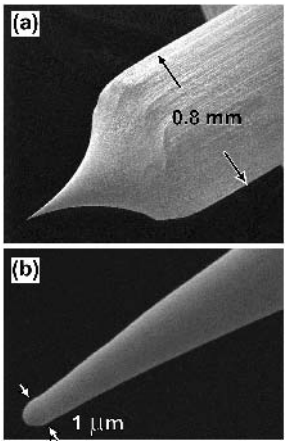

Fig. 10.1. Scanning electron micrographs of an electrochemically etched tungsten tip after flashing to $T > 2300$ K. (**a**) The overview shows the shaft of the tip (diameter: 0.8 mm) and the overall shape. (**b**) A high-resolution image reveals that the very end of the tip is blunt with a typical diameter of 1 µm

While the overall shape of the tip as displayed in the overview of Fig.10.1(a) remains almost unaffected by the high-temperature treatment, the high-resolution image of Fig.10.1(b) reveals that the tip diameter is increased to 1 μm probably due to the melting of the tip apex. In the next preparation step, the tips are coated by a thin layer of ferromagnetic material. With respect to the layer thickness several points have to be considered. On one hand, the thickness of the ferromagnetic coating should be minimized in order to reduce the tip's stray field, which might destroy the intrinsic domain structure of the sample. On the other hand, the film thickness should be well above the critical value for the onset of ferromagnetism. Additionally, in many cases, the magnetic anisotropy of a film, which determines its easy magnetization direction, varies for different film thicknesses. All these aspects have to be taken into account when choosing a suitable ferromagnetic coating. So far we have worked with probe tips that were coated by 7.5 ± 2.5 ML Fe, 8 ± 1 ML Gd, or 8 ± 1 ML GdFe. As we will show below, in general an in-plane magnetic contrast is obtained with the Fe tip, while the Gd and the GdFe tips are sensitive to the out-of-plane component of the sample's spin polarization. This fact may surprise since it might be expected that the elongated shape of the tip, as shown in Fig. 10.1(a), leads to a dominant contribution of the shape anisotropy. We have, however, shown in Fig. 10.1(b) that the tip diameter exceeds the film thickness by about three orders of magnitude. We believe that this causes material parameters like the interface and surface anisotropies to dominate the easy magnetization direction of magnetic thin film probe tips.

In our approach, tunneling spectroscopy of the local density of states is another important experimental tool since it allows the separation of structural, electronic, and magnetic sample properties. It is performed by adding a small modulation (typically 20 – 30 mV at about 2 kHz) to the applied DC bias voltage and measuring the differential conductivity $\mathrm{d}I/\mathrm{d}U$ by means of lock-in technique [9].

10.3 Experiments on Gd(0001)

In the introduction of this chapter, we described the experiments performed by Tedrow et al. [1,2] on superconductor-insulator-ferromagnet planar tunnel junctions in a high external magnetic field. In the beginning, we asked ourselves whether it is possible to find a magnetic sample that exhibits an electronic structure that is equally suited to prove spin-polarized tunneling with the STM. We found that the exchange-split d-like surface state of Gd(0001) represents a good analogue to the Zeeman-split BCS-like DOS of the superconductor. While the superconductor exhibits four peaks of well-defined spin polarization, if exposed to a strong external magnetic field, the Gd(0001) surface state is exchange split into two spin parts by exchange interaction with the half-filled 4f-shell of Gd. Actually, the majority part of the surface state is occupied, and the minority part is empty, i.e., they are energetically positioned below and above the Fermi level, respectively. Since photoemission spectroscopy (PES) and inverse (I)PES are sensitive only to electronic states below or above the Fermi level, respectively, a combined PES and IPES experiment is necessary to detect both spin parts. Such an experiment has been performed by Weschke and coworkers [10]

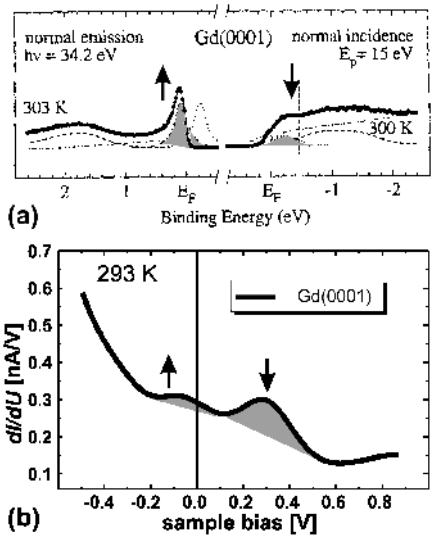

Fig. 10.2. (**a**) Photoemission and inverse photoemission spectrum of the exchange-split surface state of Gd(0001) showing the majority and the minority spin parts just below and above the Fermi level, respectively. (**b**) Tunneling spectra taken with the STM tip positioned above a Gd(0001) island. The double-peak structure represents the surface state

and is shown in Fig. 10.2(a). Since, however, the bias voltage between the sample and the tip of an STM can be tuned from positive to negative values or vice versa in a spectroscopic measurement, both empty, as well as occupied sample states, can be detected in a single experiment. Indeed, the tunneling spectrum shown in Fig. 10.2(b) exhibits two peaks at sample bias voltages of $U = -0.1\ V$ and $U = +0.3\,\mathrm{V}$ representing the occupied and empty part of the surface state, respectively. Below the Curie temperature $T_C = 293\,\mathrm{K}$, the majority and minority characters of theses states have been confirmed by spin-resolved measurements [11, 12].

As schematically represented in Fig.10.3(a) and (b), spin-polarized tunneling should lead to a striking asymmetry in the tunneling spectra: the $\mathrm{d}I/\mathrm{d}U$ signal of the particular part of the surface state being parallel to the magnetization of the tip is expected to be enhanced, while the $\mathrm{d}I/\mathrm{d}U$ signal of the peak being antiparallel to the tip is reduced. Indeed, we could observe this expected behavior experimentally with the STM. In order to minimize the field strength required for switching the magnetization direction of the sample, we have evaporated Gd on the W(110) substrate held at elevated temperature ($T = 530\,\mathrm{K}$). As can be seen in the inset of Fig. 10.3(c) this preparation procedure results in the growth of isolated Gd islands. These islands exhibit an extraordinary low coercivity of about 1.5 mT [13]. Such a small field strength can easily be reached even by coils placed outside the UHV chamber.

Since thin Gd(0001) films exhibit an in-plane anisotropy, we have used an Fe-coated probe tip for this experiment. After inserting the Fe-coated tip into the tunnel-

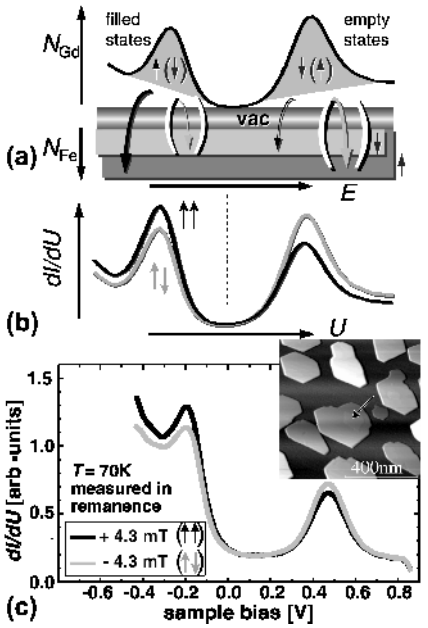

Fig. 10.3. (**a**) The principle of SP-STS using a sample with an exchange split surface state, e.g., Gd(0001), and a magnetic Fe tip with a constant spin polarization close to E_F. Due to the spin-valve effect (see Chap. 9), the tunneling current of the surface state spin component being parallel to the tip is enhanced compared with the opposite spin direction. (**b**) This should lead to a reversal in the $\mathrm{d}I/\mathrm{d}U$ signal at the peak position of the surface state upon switching the sample magnetically. (**c**) Exactly this behavior could be observed in the tunneling spectra measured with the tip positioned above an isolated Gd island (see arrow in the inset)

ing microscope, it was magnetized by applying the maximum possible field that could be produced by the coils, i.e., $\mu_0 H \approx +10\,\mathrm{mT}$. Then the sample was inserted into the sample holder, cooled down to $T = 70\,\mathrm{K}$, and magnetized by a field of $+4.3\,\mathrm{mT}$. Subsequently, 128 tunneling spectra were measured in remanence with the tip positioned above the Gd, island marked by an arrow in the inset of Fig. 10.3(c). Then the tip was retracted from the sample surface by about 200 nm, and the direction of the magnetic field was reversed ($\mu_0 H \approx -4.3\,\mathrm{mT}$). After bringing tip and sample into tunneling distance again, another 128 spectra were measured in remanence above the identical island. This procedure was repeated several times. As can be seen in the averaged $\mathrm{d}I/\mathrm{d}U$ spectra of Fig. 10.3(c), the occupied part of the exchange-split surface state is enhanced after the application of a positive field, i.e., with tip and sample magnetized parallel, while the empty part of the surface state is reduced and vice versa. This observation is in accordance with the expected behavior for spin-polarized tunneling.

Fig. 10.4(a) shows two tunneling spectra that have been measured with a Fe-coated probe tip on two adjacent Gd(0001) domains, named #1 and #2, being separated by a domain wall. Since the sample is chemically homogeneous, the differences between both spectra must be caused by spin polarized tunneling. Obviously, the

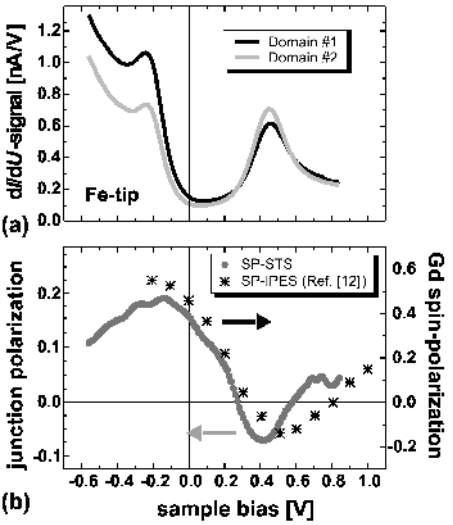

Fig. 10.4. (**a**) Tunneling spectra as measured with a Fe-covered probe tip above adjacent domains. An asymmetry of the $\mathrm{d}I/\mathrm{d}U$ signal between the empty and filled parts of the surface state can clearly be recognized. In contrast, variations in the $\mathrm{d}I/\mathrm{d}U$ signal when measured with a pure W tip are always symmetric. (**b**) Spin polarization of the tunneling current between an Fe-covered probe tip and the Gd(0001) surface at $T = 70\,\mathrm{K}$ compared to spin-polarized inverse photoemission data of Gd(0001) measured at $T = 130\,\mathrm{K}(*)$ by Donath et al. (see [12])

largest difference between both spectra, which determines the spin polarization of the tunnel junction, does not occur at the Fermi level ($U = 0\,\mathrm{V}$), but close to the position of the Gd(0001) surface state. We can calculate the spin polarization P of the tunnel junction as formed by both magnetic electrodes, tip and sample, at any energetical position around E_F by dividing the difference of the spectroscopic signal measured on both domains through the sum:

$$P = \frac{\mathrm{d}I/\mathrm{d}U_{\#1} - \mathrm{d}I/\mathrm{d}U_{\#2}}{\mathrm{d}I/\mathrm{d}U_{\#1} + \mathrm{d}I/\mathrm{d}U_{\#2}}. \tag{10.1}$$

The result is plotted in Fig. 10.4(b). Based on the observation that the spin polarization of the tunnel junction exhibits extreme values at $U = -0.13\,\mathrm{V}$ and $U = 0.42\,\mathrm{V}$, i.e., around the peak position of the minority surface state, we can conclude that – in contrast to the behavior of planar tunnel junctions with an oxide barrier for which the spin polarization was found to decrease monotonically with increasing bias voltage – surface states are of great importance for the strength of the observed magnetic signal in vacuum tunneling experiments. For comparison, Fig. 10.4(b) also shows the spin polarization of homogeneous, approximately 30 ML thick Gd(0001) films grown on W(110) as determined by means of spin-resolved inverse photoemission spectroscopy (SP-IPE) [12]. An excellent overall qualitative agreement can be recognized. Both SP-STS and SP-IPE data exhibit a positive spin polarization P on both sides of the Fermi level; P vanishes at about 300 meV and

changes sign at around $U = +0.5$ V. However, the polarization of the tunnel junction is found to be about a factor of 2.5 smaller than the Gd spin polarization as determined by SP-IPE. This difference is probably caused by the finite polarization of the second electrode, i.e., the Fe-coated probe tip.

10.4 Domain and Domain-Wall Studies on Ferromagnets

In the previous section, we described our experiments on Gd(0001), a sample which is particularly suitable for the demonstration of spin-polarized scanning tunneling spectroscopy because of its extraordinary electronic properties, i.e. the existence of an exchange-split surface state. However, almost nothing was known about the magnetic domain structure of Gd(0001) thin films on W(110) before our study [14]. In order to overcome this drawback we looked for a sample with a well-defined and previously known domain structure.

We found that Fe nanowires prepared on stepped W(110) substrates fulfill this condition. Fe nanowires have been intensively studied with a large variety of experimental methods. Especially at coverages between one and two monolayers, interesting magnetic properties were reported. For example, combining longitudinal and polar Kerr-effect measurements, an onset of perpendicular magnetization was found for Fe coverages $\Theta > 1.1$ ML. Generally, the coverage range between 1.4 and 1.8 ML Fe/W(110) is characterized by magnetic saturation at relatively low external perpendicular fields combined with the absence of a hysteresis, i.e., zero remanence. These experimental results have been interpreted as the manifestation of perpendicularly magnetized Fe double-layer (DL) stripes that prefer to occupy a demagnetized ground state by antiparallel dipolar coupling, i.e., by periodically changing the magnetization direction between adjacent DL stripes [15].

Figure 10.5(a) shows an STM image of a surface that was prepared following the recipe of Elmers, Gradmann, and coworkers [15], i.e., by deposition of 1.5 ML Fe on a stepped W(110) substrate held at elevated temperature ($T \approx 520$ K). In our case, the substrate is miscut by about 1.6°, which results in an average terrace width of 9 nm. Adjacent terraces are separated by steps of monatomic height. It is well-known that at submonolayer coverage these experimental parameters lead to the Fe decoration of substrate step edges, the so-called step-flow growth mode. After the completion of the first ML, the second atomic layer grows in a similar manner. As schematically represented in Fig. 10.5(b), the substrate is finally covered by stripes of alternating Fe nanowires of ML and DL coverage. According to the model of Elmers and Gradmann, the Fe DL nanowires are alternatingly magnetized up and down, resulting in a magnetic period that amounts to twice the structural period given by the average terrace width, i.e., about 18 nm. As schematically represented in Fig. 10.5(c), this antiparallel order is a consequence of the dipolar coupling that reduces the stray magnetic field of the perpendicularly magnetized Fe double layer. At domain walls the double layer may be locally magnetized along the hard magnetic axis, i.e., in-plane. Details of the magnetic structure, however, remained unclear. Since, e.g., the typical domain wall width of 180° amounts to about 100 nm [16], it

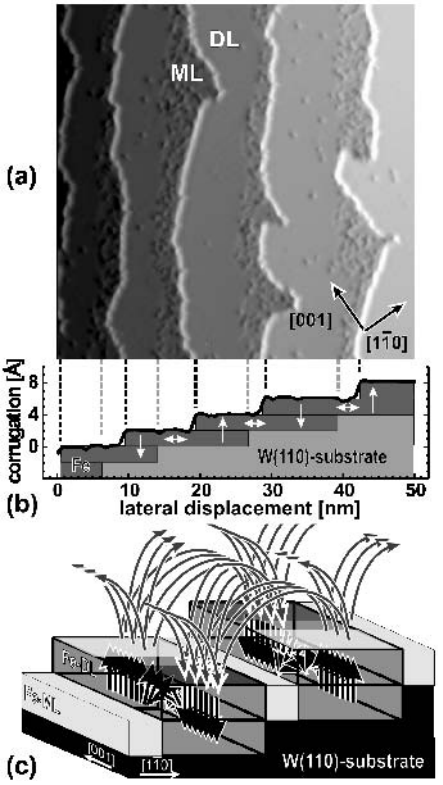

Fig. 10.5. (**a**) Topographic STM image (scan range: 50 nm × 50 nm) of 1.6 ML Fe/W(110) after annealing to 450 K. (**b**) Line section measured at the bottom edge of the STM image. The local coverage alternates between one and two atomic layers. White arrows symbolize the easy magnetization directions of the mono- and double layers, i.e., in-plane and perpendicular to the surface, respectively. (**c**) According to Elmers et al. [15], adjacent perpendicularly magnetized double-layer stripes exhibit an antiparallel dipolar coupling. Within domain walls, the Fe double layer on W(110) locally exhibits an in-plane magnetization

was controversially discussed whether in an ultrathin magnetic film a spin rotation can occur on a lateral scale of a few nanometers.

Before a sample surface can be studied by means of SP-STS, the electronic structure of the sample has to be investigated with non-magnetic tips. Figure 10.6(a) shows typical tunneling spectra of Fe on W(110) at mono- and double layer coverage as measured with a W tip. While the monolayer exhibits a peak at $U = +0.4\,\mathrm{V}$, an even stronger peak at $U = +0.7\,\mathrm{V}$ was found to be characteristic of the double layer. Besides some variations at structural dislocation sites, we found the spectra to be identical for different mono- and double layer Fe nanowires within the accuracy of our measurement. In contrast, two different types of spectra were found for the Fe DL nanowires as soon as magnetic tips were used, as shown in Fig. 10.6(b) and

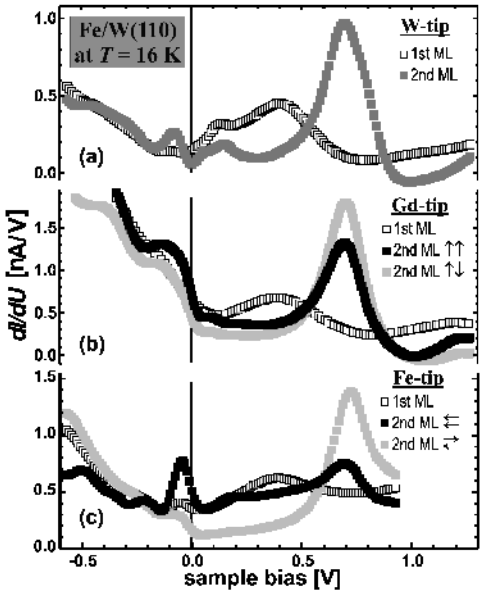

Fig. 10.6. Tunneling spectra of Fe/W(110) at mono- and double layer coverage as measured with a (**a**) nonmagnetic W tip and with a magnetic (**b**) Gd-coated and (**c**) a Fe-coated tip. With both magnetic tips we find an additional variation for the spectra of the double layer. This variation is caused by spin-polarized tunneling in magnetic domains (**b**) and domain walls (**c**)

(c) for Gd- and Fe-coated probe tips, respectively. This additional variation is caused by spin-polarized tunneling between both magnetic electrodes, i.e., tip and sample, depending on their relative magnetization directions (parallel or antiparallel). As we will show in the following, Gd tips are magnetized along the tip axis, which results in a *domain* contrast in an SP-STS experiment on the perpendicularly magnetized Fe double layer on W(110). In other words, the two different types of spectra are caused by a tip that is magnetized parallel to one domain (↑↑) and antiparallel to the other domain (↑↓). In contrast, Fe tips are magnetized perpendicular to the tip axis, which makes them sensitive to the in-plane component of the sample magnetization. Consequently, a magnetic contrast is observed when the tip is positioned above *domain walls* of the Fe double layer. Again, in the center of a domain wall the sample magnetization may be parallel or antiparallel to the tip magnetization.

Obviously, the size and the sign of the spin contrast strongly depends on the bias voltage. The Gd tip used in Fig. 10.6(b), for example, gives high contrast at the DL peak position, i.e., at $U = +680\,\mathrm{mV}$. At $U < +500\,\mathrm{mV}$ and $U > +850\,\mathrm{mV}$, the contrast inverts, as indicated by the crossing of the curves of parallel and antiparallel magnetization. The data of Fig. 10.6(c), which have been measured with a Fe-coated tip, exhibit an additional contrast inversion at $U < -0.2\,\mathrm{V}$. In our experience, the voltage at which maximal spin contrast is achieved varies between different tip preparation cycles [17]. This is probably caused by the dependence of the spin-

dependent electronic structure of the STM probe tips on the shape and the chemical composition of the cluster forming the apex of the tip.

It is very time-consuming to measure full tunneling spectra at every pixel of the image (typically 20 h for each image). Therefore, we have reduced the measurement time (to about 20 min) by scanning the sample at one particular bias voltage that, according to the spectra, is expected to give high magnetic contrast. Figure 10.7(a) and (b) show the simultaneously recorded topographic and spectroscopic $\mathrm{d}I/\mathrm{d}U$ signal, respectively, of 1.8 ML Fe/W(110), as recorded with a Gd-coated tip at $U = 0.7$ V. Since the Fe monolayer exhibits a lower differential conductivity $\mathrm{d}I/\mathrm{d}U$ at this particular bias voltage (cf. Fig. 10.5), it appears black. Due to the locally varying electronic properties, the dislocation lines in the Fe-double layer that point along the [001] direction show up as dark stripes [18]. However, there is an additional variation of the $\mathrm{d}I/\mathrm{d}U$ signal along the Fe double-layer stripes. It is caused by spin-polarized tunneling between the magnetic tip and the sample. As we have verified by the application of an external magnetic field pointing along the surface normal [19], Fig. 10.7(b) shows an out-of-plane contrast, i.e., the Gd-coated probe tip is sensitive to the perpendicular component of the spin polarization. One clearly recognizes a stripe domain pattern running along the [1$\underline{1}$0]-direction. The periodicity amounts

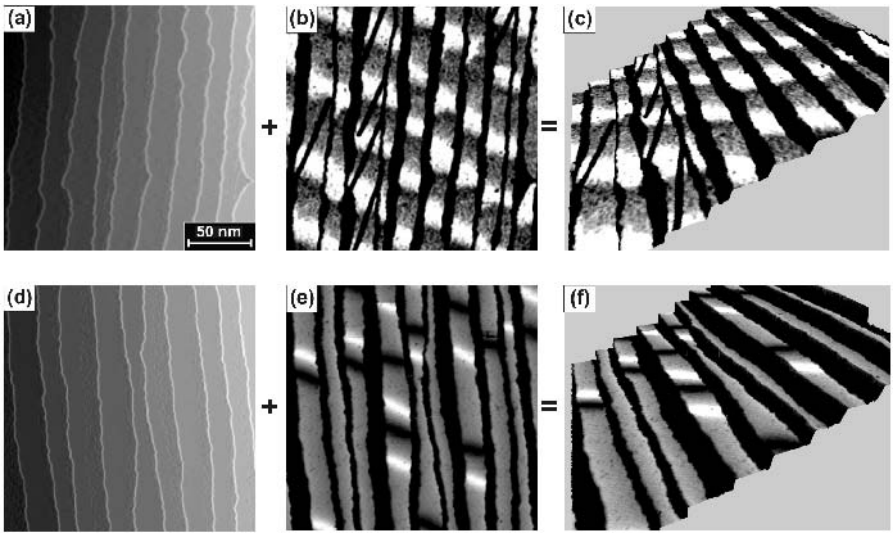

Fig. 10.7. (**a**) STM topograph and (**b**) magnetic $\mathrm{d}I/\mathrm{d}U$ signal of 1.6 ML Fe/W(110), as measured with a Gd-coated tip showing the domain structure of perpendicularly magnetized double-layer Fe nanowires. The sample exhibits a stripe domain phase with domains running along the [1$\underline{1}$0]-direction. (**c**) Rendered perspective topographic image taken from the data in (**a**) combined with a gray-scale representation of the magnetic $\mathrm{d}I/\mathrm{d}U$ signal taken from (**b**). (**d**)–(**f**) Same as (**a**)–(**c**), but measured with a Fe-coated tip being sensitive to the in-plane component of the magnetization, thereby giving domain wall contrast on this particular sample. All data were measured at a sample bias voltage $U = 0.7$ V

to approximately 50 nm. Since both the topographic, as well as the magnetic dI/dU signal have been measured simultaneously at the same position of the sample surface, we can compose a rendered three-dimensional surface contour that is superimposed by the magnetic signal in a gray-scale representation. This is shown in Fig. 10.7(c) and allows an intuitive understanding of structural and magnetic properties of the investigated surface on a single-digit nanometer scale.

So far we have shown that Fe nanowires at a total coverage just below two atomic layers exhibit a stripe domain phase, i.e., the magnetization periodically changes between up and down along a single double-layer stripe. This implies, however, that numerous domain walls must be present. Inside the domain wall the magnetization continuously rotates between either perpendicular magnetization directions. Therefore, in the center of the wall the magnetization must point along the hard axis of the Fe double layer. However, this rotation may take place in two different rotational directions, i.e., either clockwise or counter-clockwise. Is it possible to distinguish between those two cases? We found that this can indeed be accomplished by using Fe-coated tips. Figure 10.7(d) and (e) again show the simultaneously recorded topographic and spectroscopic dI/dU signals, respectively, of a similar sample as, imaged in Fig. 10.7(a)–(c). In contrast to the data measured with the Gd tip, the magnetically induced variation of the dI/dU signal is now localized to narrow lines running along the [1$\underline{1}$0]-direction. We identify these bright and dark lines as domain walls that exhibit opposite senses of rotation. Since, however, we currently cannot control the in-plane magnetization direction of our tips, we are not able to judge which part of the line, dark or bright, corresponds to (counter)clockwise rotating domain walls.

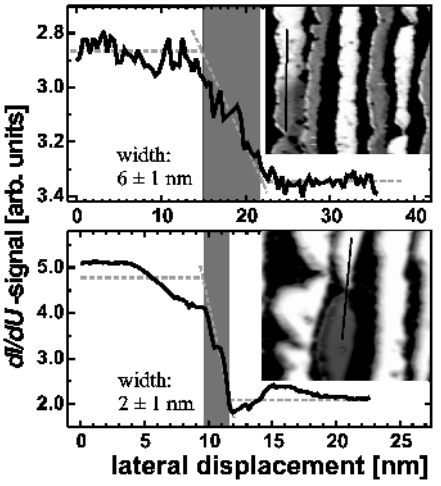

Fig. 10.8. Line sections showing the change of the dI/dU signal when crossing a domain wall located in a smooth (*upper panel*) or constricted (*lower panel*) Fe double-layer stripe. Maps of the dI/dU signal are shown as insets. The positions at which the line sections were drawn are marked by black solid lines

The development of spin-polarized STM/STS was motivated by the hope that the high spatial resolution of STM can be combined with magnetic sensitivity. Although we will show later on that even atomic resolution can be obtained by SP-STM, we would like to demonstrate here the gain in resolution made possible by SP-STS already by showing line profiles drawn across some domain walls in Fe double-layer nanowires. In Fig. 10.8, we have plotted two section lines crossing a domain wall in a smooth (top panel), as well as in a constricted Fe nanowire (bottom panel). While the width of the former domain wall amounts to $w = 6 \pm 1$ nm, the latter is much narrower ($w = 2 \pm 1$ nm). Both values of the domain wall width were well beyond the resolution limit of other magnetic imaging techniques. Although these domain walls extend over less than 20 lattice sites, we found that they can still be interpreted in the framework of micromagnetic continuum theory [20] by $w = 2(A/k)^{1/2}$, with the exchange stiffness A and the first order anisotropy constant k [21]. The mechanism that leads to the narrowing of the domain wall in the constriction has recently been described by Bruno [22].

10.5 Surface Spin-Structure Studies of Antiferromagnets

The exchange bias effect, i.e., the pinning of a ferromagnet due to exchange coupling to an antiferromagnet, has been discovered as early as 1957 [23]. As already pointed out in Chaps. 2 and 7, antiferromagnets have recently been of great economic interest due to their application in planar tunnel junctions. This has triggered numerous studies on details of the domain structure of antiferromagnetic surfaces and the coupling mechanism between the antiferromagnet and the ferromagnet [24]. However, due to the fact that the magnetic moments of antiferromagnets cancel out on lateral dimensions above the atomic scale, the measurement of their magnetic properties is particularly challenging. Therefore, a magnetic imaging technique that combines high lateral resolution with high surface sensitivity is desirable, and its availability may lead to a better understanding of antiferromagnetic surfaces and of details of the exchange-bias effect.

Antiferromagnetic chromium has been intensively investigated in the past and is still the subject of numerous experimental and theoretical studies [25, 26]. Several magnetic effects, e.g., the giant magnetoresistance effect and the interlayer exchange coupling, have been discovered in Fe/Cr multilayers. In spite of its importance, little was known about the domain structure of Cr.

Cr exhibits a transverse and a longitudinal spin-density wave below the Néel temperature $T_N = 311$ K and the spin-flip temperature $T_{sf} = 121$ K, respectively. The spin-density wave may propagate along three equivalent [001]-directions, leading to a ferromagnetic coupling within single (001)-planes, but to an antiferromagnetic coupling between adjacent (001)-planes. Although it was shown theoretically that even the (001) *surface* of Cr couples ferromagnetically and exhibits an enhanced magnetic moment [27], no net magnetic moment could be found by spin-resolved photoemission [28]. As first pointed out by Blügel et al. [29], this is caused by the fact that surfaces cannot be prepared atomically flat. Instead, a real surface always

exhibits steps that separate the different atomically flat terraces from each other. Thereby, different (001)-planes with opposite magnetization directions are exposed to the surface, leading to the so-called "topological antiferromagnetism" of the Cr(001) surface. Typically, these terraces have a width of about 10 nm up to several hundreds of nanometers. Furthermore, the magnetization of the first subsurface layer points opposite to the surface. Therefore, all experimental methods with insufficient lateral resolution (> 10 nm) or surface sensitivity (> 1 ML) average over regions of opposite magnetization, which leads to their compensation.

SP-STM/STS does not suffer from these limitations. Both the lateral resolution as well as the surface sensitivity are well beyond the requirements mentioned above. Indeed, by using constant-current SP-STM Wiesendanger et al. [30] found the first experimental evidence of topological antiferromagnetism on the Cr(001) surface. In this experiment, CrO_2 tips with a high degree of spin polarization were successfully used to detect periodic alternations of the measured mono-atomic step heights in constant-current images. The deviations of the measured step height values from the topographic mono-atomic step height could be related to the effective spin polarization of the tunnel junction.

A significant drawback of this experimental approach was, however, the superposition of topographic and magnetic structure information. To solve this problem, we have performed spectroscopic measurements on Cr(001) similar to those previously described for Fe nanowires (cf. Fig. 10.6). Figure 10.9(a) shows an averaged spectrum measured with a nonmagnetic W tip. A peak which is known to be d-derived and spin polarized [31] can be recognized very close to the Fermi level ($U = 0$ V). The inset shows the topography and a map of the $\mathrm{d}I/\mathrm{d}U$ signal at the peak position. The correlation of both images reveals that the differential conductivity does not change across a step edge if the measurement is performed with a nonmagnetic tip. As shown in Fig. 10.9(b), spatial variations of the $\mathrm{d}I/\mathrm{d}U$ signals could only be detected after using Fe-coated tips that exhibit the required in-plane anisotropy: Due to different relative magnetization directions between the tip on one side and terraces A and B on the other side, the $\mathrm{d}I/\mathrm{d}U$ signal changes at the position of the step edge.

Again, we can reduce the measurement time considerably by restricting ourselves to a single bias voltage, which gives high magnetic contrast. The data presented in Fig. 10.9(b) might suggest that a high magnetic contrast can be achieved at the Cr(001) surface state peak position, i.e., very close to the Fermi level. We have, however, to take into account that the tip-sample distance is not constant, but – as a result of the constant-current mode of operation – depends on the local differential conductivity, which is not only an intrinsic property of the sample surface but which in spin-polarized experiments is also influenced by the relative magnetization direction of tip and sample. If Cr(001), which is chemically homogeneous, is scanned in the constant-current mode with a magnetic tip at a bias voltage corresponding to the energetic position close to the surfaces state, the tip-sample distance is increased (decreased) above Cr terraces magnetized (anti)parallely with respect to the tip. As already mentioned above, this variation of the tip-sample distance shows up as deviations of the measured step height values from the topographic step height [30, 32]. This, however, leads to a strong reduction of the variation of the differential conductivity

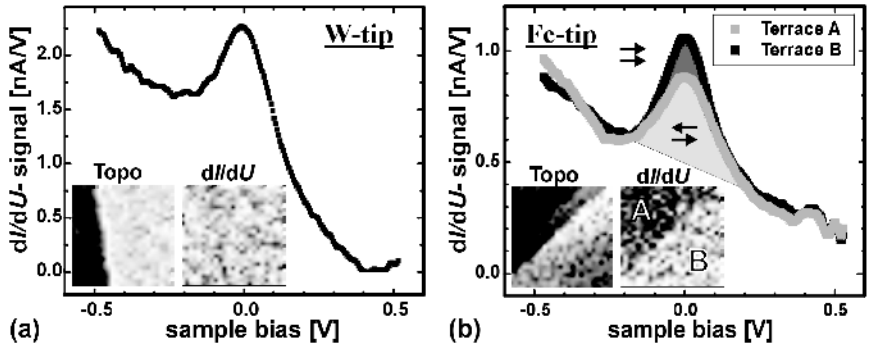

Fig. 10.9. Typical tunneling spectrum of Cr(001) as measured (**a**) with a non-coated W tip and (**b**) with a Fe-coated tip. All spectra are dominated by a strong peak at $U = -20\,\mathrm{mV}$, which represents the *d*-like surface state [31]. The insets show the topography (left) and maps of the $\mathrm{d}I/\mathrm{d}U$ signal at the surface state peak position (right). In both cases, the topography shows two atomically flat terraces that are separated by a monoatomic step edge. While the spectra measured with the W tip are identical on both terraces, the spatially resolved $\mathrm{d}I/\mathrm{d}U$ signal, as measured with the Fe-coated tip, reveals significant differences between the two terraces due to the vacuum-tunneling magnetoresistance effect

$\mathrm{d}I/\mathrm{d}U$ above oppositely magnetized Cr(001) terraces. A high (magnetic) $\mathrm{d}I/\mathrm{d}U$ contrast can only be achieved if the spin polarization of the (energy-integrated) tunnel current differs from the spin polarization of the electronic states at the energy that corresponds to the applied bias voltage U [35]. In our experience, on Cr(001), the highest $\mathrm{d}I/\mathrm{d}U$ contrast is obtained at $U \approx \pm(250 \pm 50\,\mathrm{mV})$. Figure 10.10(a) shows the defect-free topography of a Cr(001) surface measured with a Fe-coated tip at $U \approx -290\,\mathrm{mV}$. Figure 10.10(b) reveals that the nine atomically flat terraces are separated by steps of monoatomic height. At this bias voltage, the measured step height is equal to the topographic step height for all step edges. According to Blügel's model, this topography should lead to a magnetization that alternates between adjacent terraces. This is indeed observed experimentally in the magnetic $\mathrm{d}I/\mathrm{d}U$ signal that alternates from terrace to terrace between high (bright) and low (dark), thereby proving the idea of "topological antiferromagnetism" [Fig. 10.10(c)].

Figure 10.11 shows the topography of a different sample that exhibits two screw dislocations within the scan range. They are marked by arrows. In a "topological antiferromagnet", the presence of screw dislocations leads to magnetic frustrations. As can be recognized in the magnetic image of Fig. 10.11(b), in this particular case, a domain wall is created at one dislocation and annihilated at the other dislocation. Again, a three-dimensionally rendered representation of the measured data can be generated on the basis of the measured topography and $\mathrm{d}I/\mathrm{d}U$ signal.

As indicated by two lines in Fig. 10.11(b), we have drawn line profiles of the $\mathrm{d}I/\mathrm{d}U$ signal across the domain wall in two adjacent Cr terraces. The result is plotted in Fig. 10.12. We found that the line profiles can be fitted nicely by a tanh function, which describes a 180° wall in the framework of micromagnetic theory [20]:

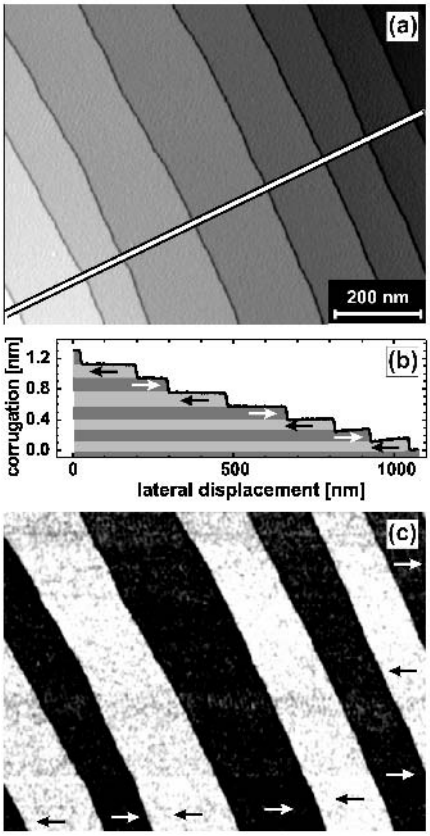

Fig. 10.10. (**a**) STM topograph of the Cr(001) surface (scan range: 800 nm × 600 nm). (**b**) The line section that has been drawn along the white line reveals that the terraces are separated by step edges of monatomic height. (**b**) According to Blügel's model of "topological antiferromagnetism", [29] this topography should lead to a surface magnetization that alternately switches between opposite directions from terrace to terrace. (**c**) In fact, using a Fe-coated probe tip alternately magnetized Cr terraces are observed by SP-STS ($U = -290$ mV)

$$y(x) = y_0 + y_{sp} \tanh\left(\frac{x - x_0}{w/2}\right), \tag{10.2}$$

where $y(x)$ is the $\mathrm{d}I/\mathrm{d}U$ signal measured at position x, x_0 is the position of the domain wall, w is the wall width, and y_0 and y_{sp} are the spin-averaged and spin-polarized $\mathrm{d}I/\mathrm{d}U$ signal, respectively.

As already mentioned above, the development of SP-STM was driven by the ultrahigh spatial resolution of STM, which allowed for the first time the study of structural and electronic properties of surfaces with atomic resolution in real space and over extended areas of the surface. It was an open question whether atomic resolution can also be achieved in a spin-sensitive measurement. The smallest magnetic structure

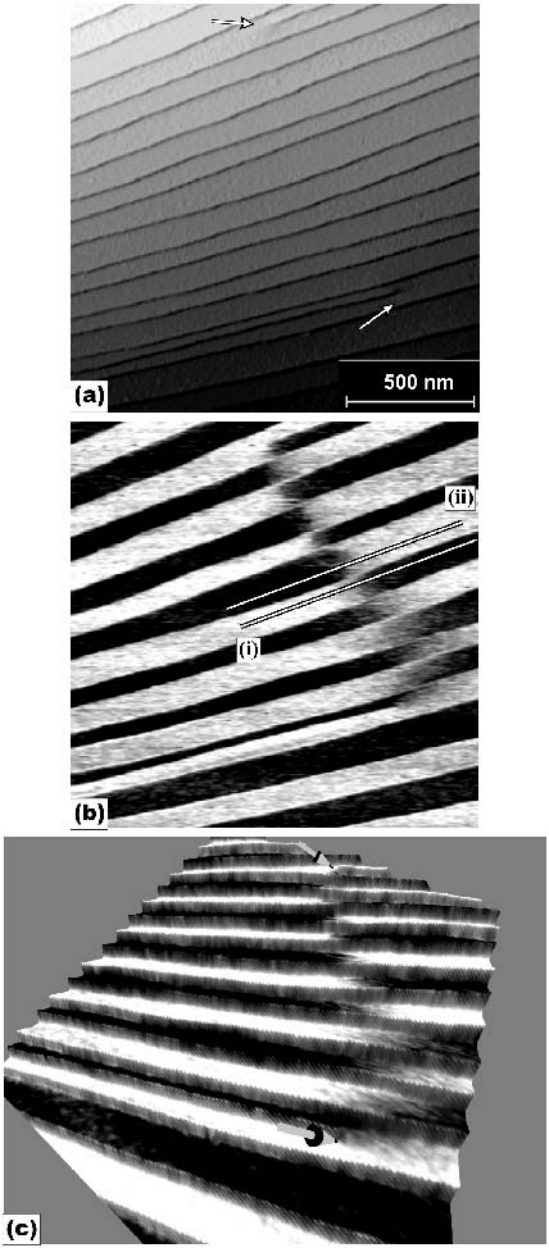

Fig. 10.11. (**a**) Topography and (**b**) $\mathrm{d}I/\mathrm{d}U$ signal at $U = 190\,\mathrm{mV}$ of a Cr(001) surface. The surface is magnetically dominated by a magnetization that alternates between adjacent Cr(001) terraces. Within the scan range of $2\,\mu\mathrm{m} \times 2\,\mu\mathrm{m}$, the sample exhibits two screw dislocations. Spin frustration leads to the formation of a magnetic domain wall between these dislocations. A line section drawn along the lines will be shown in Fig. 10.12. (**c**) Rendered perspective topographic image combined with a gray-scale representation of the magnetic $\mathrm{d}I/\mathrm{d}U$ signal

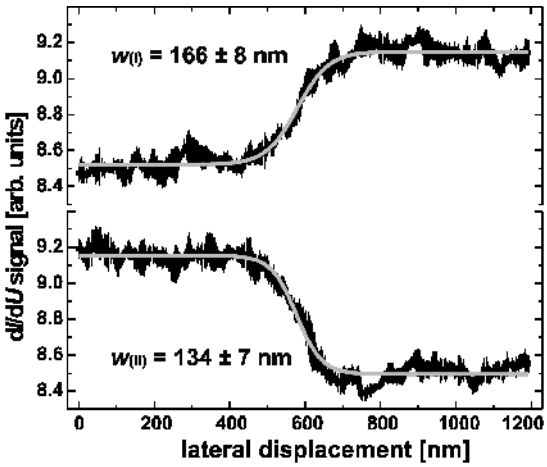

Fig. 10.12. Two domain wall profiles taken along the white lines in Fig. 10.11. The wall profiles can be fitted nicely by micromagnetic theory, resulting in domain wall widths of $w_{(i)} = 134 \pm 7$ nm and $w_{(ii)} = 66 \pm 8$ m

one can imagine is an antiferromagnetic, densely packed layer in which atoms in nearest neighbor sites exhibit opposite magnetization directions. Such a magnetic configuration was already predicted by Blügel and coworkers in 1988 [33] for several transition metal overlayers on noble-metal (111) substrates. It turned out, however, that the experimental proof of this prediction is extremely difficult. First of all, as already mentioned above, the magnetic moments of the antiferromagnetic layer cancel each other, leading to zero total magnetization on the macroscopic scale. Furthermore, the Néel temperature of that layer was unknown and probably very low. Finally, noble metals tend to intermix with transition metal adlayers, which makes their preparation almost impossible. Obviously, the first two problems can be overcome by low-temperature SP-STM. But what about the third problem? It is well-known that intermixing plays no role for refractory substrates as, e.g., tungsten (W).

In fact, in a more recent calculation, Blügel and coworkers found that a single Mn monolayer on W(110) also exhibits an antiferromagnetic ground state [34]. The typical morphology of Mn on W(110) ($\Theta = 0.68$ ML) at submonolayer coverage can be seen in the STM topograph of Fig. 10.13. It is dominated by pseudomorphically grown Mn islands of monolayer height. As long as a tungsten tip is used for the STM measurements, the experiment is not sensitive to the spin of the tunneling electron. Therefore, the opposite magnetization directions of adjacent Mn atoms cannot contribute to the tunneling current, and atomic resolution STM images should only represent the chemical unit cell. Indeed, no magnetic contribution to the experimental data can be recognized in the atomic resolution STM image of Fig. 10.14(a), which has been measured on an atomically flat Mn island on W(110) using a non-magnetic W tip. Since the electronic properties of all Mn atoms are identical, the magnetic superstructure is "ignored". The inset allows a comparison of the measured data with

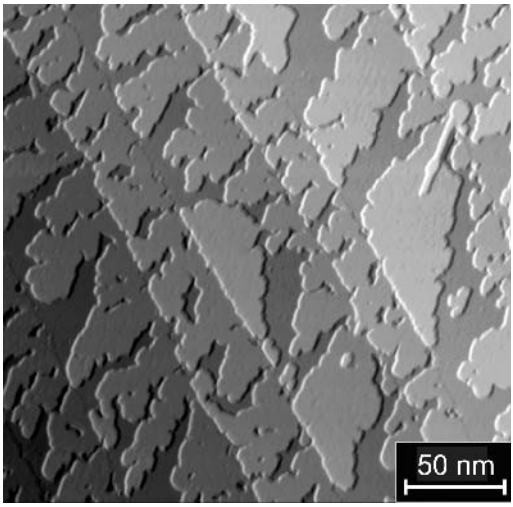

Fig. 10.13. STM topograph of 0.68 ML Mn on W(110). The morphology is dominated by pseudomorphically grown Mn islands of monolayer height

theoretically calculated atomic resolution STM images. A good qualitative agreement can be recognized.

If, however, an appropriate magnetic tip is used – due to the in-plane anisotropy of the Mn monolayer, we have used a Fe-coated tip here – the tunneling current depends on the relative magnetization direction of the tip and the sample. It has been shown theoretically for the general case [34, 35] that due to the exponential damping of large reciprocal lattice vectors, the largest magnetic superstructure will dominate the image in most cases, i.e., even if the magnetization of the tip is canted out of the plane by 80°. Figure 10.14(b) shows a high resolution STM image of 1ML Mn/W(110) obtained with a Fe tip. The scan range is the same as in Fig. 10.14(a). Instead of an atomic resolution image with a periodicity determined by the chemical unit cell, we now recognize stripes running along the [001]-direction. The periodicity perpendicular to the stripes amounts to 4.5 Å, i.e., twice the structural periodicity. The interpretation of this observation is straightforward: If the magnetic tip and the Mn rows are magnetized parallel, the tunneling current will be relatively large and, as a consequence of the constant-current mode of operation, the tip will be retracted (bright). The magnetization of all other Mn rows is antiparallel to the tip, which results in a lower tunneling current. Consequently, the tip is approached toward the surface (dark).

Nowadays, ferro- and antiferromagnetic materials are important components in high-density data storage devices. Therefore, advanced tools for microscopic characterization of the nanoscale magnetic structures are required. As pointed out previously, the investigation of antiferromagnetic surfaces is particularly difficult, as their net magnetization vanishes and many magnetically sensitive imaging techniques are not applicable. Here, spin-polarized scanning tunneling microscopy and spectroscopy

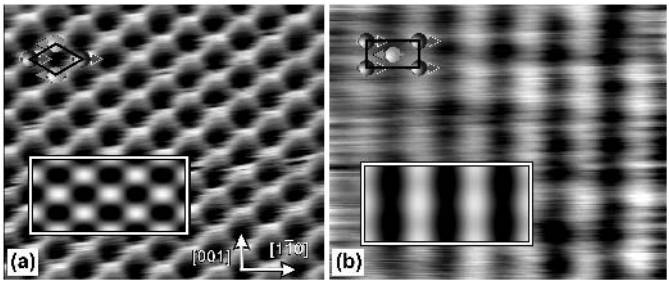

Fig. 10.14. Atomic resolution constant-current STM images measured on antiferromagnetic monolayer Mn islands on W(110) using (**a**) a nonmagnetic W tip and (**b**) a magnetic Fe tip (tunneling parameters for both images: $I = 40$ nA, $U = -3$ mV). With a W tip, the opposite magnetization direction of adjacent Mn atoms cannot be distinguished, leading to an STM image with a periodicity that is determined by the size of the chemical unit cell. In contrast, the Fe tip is sensitive to the spin of the tunneling electrons. Therefore, the periodicity of the antiferromagnetic c(2×2) unit cell shows up in (**b**)

close a gap and may allow significant contributions toward a better understanding of important physical phenomena, as, e.g., the exchange bias effect.

Conclusions

We have shown that nanostructured magnetic domains in ferromagnets, as well as antiferromagnets can be imaged by spin-polarized scanning tunneling spectroscopy (SP-STS) with unprecedented spatial resolution. The contrast mechanism of SP-STS is based on an additional variation of the measured differential conductivity $\mathrm{d}I/\mathrm{d}U$ when a magnetic tip is used. This method allows the clear and simultaneous identification and separation of structural, electronic, and magnetic surface properties. Since STS is a near-field technique, it can be operated even in strong external fields [19]. Using the constant-current mode of operation (SP-STM), we could show that atomic spin resolution on antiferromagnetic surfaces can be obtained.

Acknowledgement. We gratefully acknowledge contributions of and discussions with S. Blügel, M. Getzlaff, S. Heinze, M. Kleiber, A. Kubetzka, X. Nie, O. Pietzsch, and R. Ravlic. Financial support has been provided by the "Bundesministerium für Bildung und Forschung" and by the "Deutsche Forschungsgemeinschaft".

References

1. P.M. Tedrow, R. Meservey, and P. Fulde, Phys. Rev. Lett. **25**, 1270 (1970).
2. P.M. Tedrow and R. Meservey, Phys. Rev. B **7**, 318 (1973).
3. D.T. Pierce, Physica Scripta **38**, 291 (1988).
4. S.F. Alvarado and P. Renaud, Phys. Rev. Lett. **68**, 1387 (1992).
5. Y. Suzuki, W. Nabhan, and K. Tanaka, Appl. Phys. Lett. **71**, 3153 (1997).

6. R. Jansen, R. Schad, and H. van Kempen, J. Magn. Magn. Mat. **198–199**, 668 (1999).
7. M. Pratzer, H.J. Elmers, M. Bode, O. Pietzsch, A. Kubetzka, and R. Wiesendanger, Phys. Rev. Lett. **87**, 127201 (2001).
8. O. Pietzsch, A. Kubetzka, D. Haude, M. Bode, and R. Wiesendanger, Rev. Sci. Instr. **71**, 424 (2000).
9. R. Wiesendanger, *Scanning Probe Microscopy and Spectroscopy*, Cambridge University Press (1994).
10. E. Weschke, C. Schuessler-Langeheine, R. Meier, A.V. Fedorov, K. Starke, F. Huebinger, and G. Kaindl, Phys. Rev. Lett. **77**, 3415 (1996).
11. D. Li, J. Pearson, S.D. Bader, D.N. McIlroy, C. Waldfried, and P.A. Dowben, Phys. Rev B **51**, 13895 (1995).
12. M. Donath, B. Gubanka, and F. Passek, Phys. Rev. Lett. **77**, 5138 (1996).
13. M. Farleand and W.A. Lewis, J. Appl. Phys. **75**, 5604 (1994).
14. M. Bode, M. Getzlaff, and R. Wiesendanger, Phys. Rev. Lett. **81**, 4256 (1998).
15. H.J. Elmers, J. Hauschild, and U. Gradmann Phys. Rev. B **59**, 3688 (1999).
16. H.P. Oepen and J. Kirschner, Phys. Rev. Lett. **62**, 819 (1989).
17. M. Bode, O. Pietzsch, A. Kubetzka, and R. Wiesendanger, J. Electr. Spectr. Relat. Phenom. **114–116**, 1055 (2001).
18. M. Bode, R. Pascal, M. Dreyer, and R. Wiesendanger, Phys. Rev. B **54**, 8385 (1996).
19. O. Pietzsch, A. Kubetzka, M. Bode, and R. Wiesendanger, Science **292**, 2053 (2001).
20. A. Hubert and R. Schäfer, *Magnetic Domains*, Springer (1998).
21. O. Pietzsch, A. Kubetzka, M. Bode, and R. Wiesendanger, Phys. Rev. Lett. **84**, 5212 (2000).
22. P. Bruno, Phys. Rev. Lett. **83**, 2425 (1999).
23. W.H. Meiklejohn and C.P. Bean, Phys. Rev. **105**, 904 (1957).
24. J. Stöhr, A. Scholl, T.J. Regan, S. Anders, J. Lüning, M.R. Scheinfein, H.A. Padmore, and R.L. White, Phys Rev. Lett. **83**, 1862 (1999).
25. E. Fawcett, Rev. Mod. Phys. **60**, 209 (1988).
26. H. Zabel, J. Phys.: Cond. Matter **11**, 9303 (1999).
27. C.L. Fu and A.J. Freeman, Phys. Rev. B **33**, 1755 (1986).
28. L.E. Klebanoff, S.W. Robey, G. Liu, and D.A. Shirley, Phys. Rev B **30**, 1048 (1984).
29. S. Blügel, D. Pescia, and P.H. Dederichs, Phys. Rev. B **39**, 1392 (1989).
30. R. Wiesendanger, H.-J. Güntherodt, G. Güntherodt, R.J. Gambino, and R. Ruf, Phys. Rev. Lett. **65**, 247 (1990).
31. J.A. Stroscio, D.T. Pierce, A. Davies, R.J. Celotta, and M. Weinert, Phys. Rev. Lett. **75**, 2960 (1995).
32. M. Kleiber, M. Bode, R. Ravlic, and R. Wiesendanger, Phys. Rev. Lett. **85**, 4606 (2000).
33. S. Blügel, M. Weinert, and P.H. Dederichs, Phys. Rev. Lett. **60**, 1077 (1988).
34. S. Heinze, M. Bode, A. Kubetzka, O. Pietzsch, X. Nie, S. Blügel, and R. Wiesendanger, Science **288**, 1805 (2000).
35. D. Wortmann, S. Heinze, Ph. Kurz, G. Bihlmayer, and S. Blügel, Phys. Rev. Lett. **86**, 4132 (2001).